The New French Operational Polarimetric Radar Rainfall Rate Product

JORDI FIGUERAS I VENTURA AND PIERRE TABARY

Météo France, Toulouse, France

(Manuscript received 22 June 2012, in final form 1 March 2013)

ABSTRACT

In 2012 the Météo France metropolitan operational radar network consists of 24 radars operating at C and S bands. In addition, a network of four X-band gap-filler radars is being deployed in the French Alps. The network combines polarimetric and nonpolarimetric radars. Consequently, the operational radar rainfall algorithm has been adapted to process both polarimetric and nonpolarimetric data. The polarimetric processing chain is available in two versions. In the first version, now operational, polarimetry is only used to correct for attenuation and filter out clear-air echoes. In the second version there is a more extensive use of polarimetry. In particular, the specific differential phase K_{dp} is used to estimate rainfall rate in intense rain. The performance of the three versions of radar rainfall algorithms (conventional, polarimetric V1, and polarimetric V2) at different frequency bands (S, C, and X) is evaluated by processing radar data of significant events offline and comparing hourly radar rainfall accumulations with hourly rain gauge data. The results clearly show a superior performance of the polarimetric products with respect to the nonpolarimetric ones at all frequency bands, but particularly at higher frequency. The second version of the polarimetric product, which makes a broader use of polarimetry, provides the best overall results.

1. Introduction

Accurate rainfall estimation is fundamental for many applications in hydrology, nowcasting, and so on. Weather radars are the most adequate instruments to reveal the high-resolution spatial and temporal variation of the rainfall fields, and their potential value for quantitative precipitation estimation (QPE) was recognized since practically the beginning of the field (Marshall et al. 1947). However, radar measurements are subject to multiple uncertainty sources, which can roughly be grouped in three categories (Zawadzki 1984): 1) errors related to the radar system itself (calibration biases, antenna positioning errors, etc.), 2) errors related to the interaction between the radar signal and the environment [clutter, partial beam blocking (PBB), attenuation, etc.], and 3) ambiguity of the relation between radar measurement and surface rainfall accumulation [precipitation type, nonuniform vertical profile of reflectivity (VPR), drop size distribution (DSD) variability, etc.].

Corresponding author address: Jordi Figueras i Ventura, Centre de Météorologie Radar, Direction des Systèmes d'Observation, Météo France, 42 Av. Coriolis, 31057 Toulouse CEDEX, France.
E-mail: jordi.figueras@meteo.fr

DOI: 10.1175/JAMC-D-12-0179.1

A continuous effort by the entire weather radar community has been made in quantifying and mitigating these sources of error. A comprehensive review is out of the scope of this article, but we can cite works on ground clutter identification (Sugier et al. 2002), PBB correction (Delrieu et al. 1995), or VPR correction (Koistinen 1991; Kitchen 1997; Andrieu and Creutin 1995; Joss and Lee 1995; Germann and Joss 2002).

The first operational Météo France radar rainfall product dates from 1997. Since then, the demand by end users has resulted in an increase of both the number of radar systems and the complexity of the signal processing up to reaching the product described hereinafter (see Tabary 2007).

The recent advance of polarimetry has opened new perspectives since the extra information provided by polarimetric variables can significantly help in mitigating errors (Bringi and Chandrasekar 2001). It enables identification of the scatterers (Park et al. 2009), attenuation correction (Gu et al. 2011), and real-time retrieval of the DSD parameters (Brandes et al. 2004). Numerous polarimetric QPE algorithms have been proposed at S, C, and X band (see Ryzhkov et al. 2005; Bringi et al. 2011; Tabary et al. 2011; Figueras i Ventura et al. 2012a).

Despite the fact that the first studies on polarimetric QPE date from the 1970s [e.g., that of Seliga and Bringi

(1976)], up to very recently polarimetric radars were used mainly in the atmospheric research domain and not in the operational weather radar networks. Here are some examples (among others) to illustrate the extension toward operations: The U.S. National Weather Service is currently upgrading its S-band weather radar network to polarimetry (Cocks et al. 2012). In Europe, C-band radars are much more common. Several weather services have recently upgraded (Finish Meteorological Institute; various Italian regional services) or are upgrading (Met Office; Deutscher Wetterdienst) part or all of their weather networks (Figueras i Ventura et al. 2012b). In Japan there exists an operational X-band polarimetric radar network for weather surveillance in densely inhabited areas (Maesaka et al. 2011).

The operational deployment of polarimetry is complex: regardless of the hardware upgrade, accurate polarimetric-variable monitoring techniques have to be implemented, personnel and end users have to be trained, the coexistence of polarimetric and nonpolarimetric radars has to be dealt with, and so on. More important, the theoretical capabilities of polarimetry have to be revisited, taking into account realistic assumptions on the quality of polarimetric variables estimated by operational scanning radars.

The first Météo France polarimetric radar was installed in 2004 in Trappes, near Paris. The installation was followed by a long period of research and development [see Figueras i Ventura et al. (2012a) for an overview], which finally resulted in a first version of a polarimetric preprocessing chain introduced into operations in February 2012. This first version basically corrects for precipitation-induced attenuation the radar reflectivity Z_h using the differential phase ϕ_{dp}.

The encouraging results obtained led to the development of a second version of the polarimetric radar rainfall product, which further enhances the use of polarimetric data. In a first step, a long-term data quality analysis of the S- and C-band radars was undertaken to verify the feasibility of using polarimetric variables for quantitative measurements. It followed a test in semi-ideal conditions (PBB-free areas, rain-only events, and single tilt) at C band of several polarimetric QPE algorithms to determine the optimal one. A hybrid reflectivity–rainfall (Z–R) and specific differential phase (K_{dp})–R algorithm was considered the best choice. The research is described in detail in Figueras i Ventura et al. (2012a). This algorithm is implemented in the second version of the operational polarimetric radar rainfall product.

This paper objectively evaluates the performance of each radar rainfall product: monopolar and the first and second polarimetric versions at the three frequency bands used at Météo France: S, C, and X. It therefore provides useful information on what improvement on performance can be expected from the operational use of polarimetry and valuable insight on the added capability of polarimetry at each frequency band.

The paper is structured as follows: Section 2 summarizes the current operational radar rainfall products for both single-polarization and polarimetric radars. Section 3 describes the second version of the polarimetric radar rainfall product. Section 4 analyzes the differences between the new and old quality indexes (QI) used to combine the radar data. Section 5 analyzes the results of the objective evaluation of the three products at S, C, and X band performed using rain gauge data. Conclusions and future developments are discussed in section 6.

2. Current operational radar rainfall product

The current operational weather radar network (in June 2012) at metropolitan France is composed of 24 radars. Most of the radars are C band, but there are six S-band radars in the south of France, which, because of the Mediterranean climate, are more exposed to extreme precipitation events (Didier et al. 2012). At the moment there are 13 polarimetric radars in the network, 11 at C band and 2 at S band. It is expected that by 2020 all radars in the network will be polarimetric. The exploitation mode of each radar consists of a supercycle repeated every 15 min divided into 5-min cycles. In each cycle, from four to six scans at different elevation angles (depending on the orography) are performed. The elevation angles range from 0.4° up to 15°. In addition, all polarimetric radars have a vertically pointing scan for calibration purposes. The lowest tilts, optimal for hydrological applications, are revisited every 5 min.

In addition to the operational radars, there are two X-band radars in the French Alps in the framework of the Risques Hydrométéorologiques en Territoires de Montagnes et Mediterranéens (RHYTMME) project (Kabeche et al. 2012). These radars are used as gap fillers. Within the RHYTMME project a network of four radars is planned. At the moment Météo France has deployed one of these radars. The other one is a preexisting "HYDRIX" radar owned by Le Centre National de la Recherche Scientifique (CNRS) and operated by "NOVIMET." Because of the coexistence of polarimetric and nonpolarimetric radars in the network, the operational radar rainfall products have two operational modes: one that makes use of polarimetry and one that does not.

a. Operational radar rainfall product

The processing chain of the conventional single-polarization radar was described in detail in Tabary (2007). A few changes have been introduced since that paper was published. For convenience we summarize in

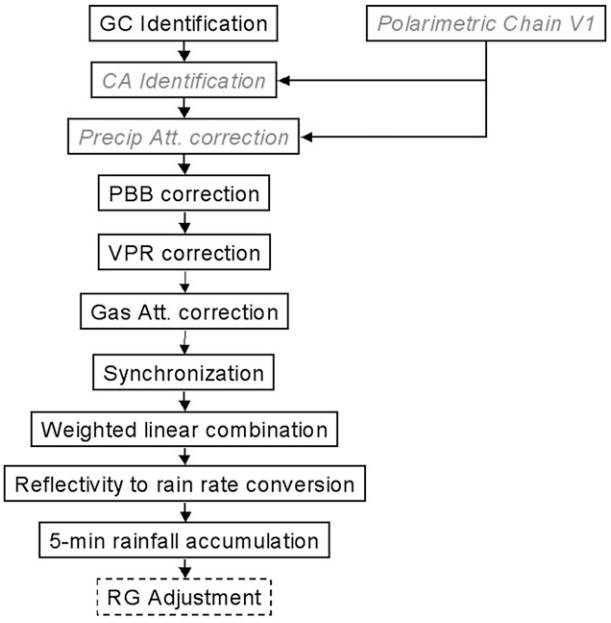

FIG. 1. Flow diagram of the operational radar rainfall product. Polarimetric modules are identified by the gray italics.

the following the main processing steps. The modules introduced since the publication of Tabary (2007) are discussed in more detail. The flow diagram of the algorithm can be seen in Fig. 1. This figure includes the polarimetric modules introduced in the first version of the polarimetric rainfall product that are further discussed in section 2b. The processing is performed on Z_h data in Cartesian coordinates with 1-km^2 pixel resolution, obtained at each scan. During the processing, a QI matrix (1 for perfect measurement and 0 for a not-usable pixel) for each scan is generated.

1) CLUTTER IDENTIFICATION

In Tabary (2007) ground clutter (GC) identification is performed exclusively based on a threshold on the pulse-to-pulse fluctuation of the radar reflectivity σ_z (Sugier et al. 2002). The threshold level σ_{z0} depends on the measurement conditions. In areas of permanent GC, the threshold is more restrictive. A new condition has been added whereby the threshold is also more restrictive if Doppler velocity is very low and hence likely to correspond to GC. Moreover the pixels adjacent to a pixel identified as GC are further analyzed. If no pixel adjacent to those pixels is valid they are classified as well as GC. Otherwise their reflectivity value is substituted by the average reflectivity of the surrounding valid pixels. Additionally, pixels that are statistically contaminated by windmill echoes or sea clutter echoes or that have a Z_h texture above a threshold are classified as GC.

2) PBB CORRECTION

The Z_h value is corrected according to a PBB static map. In addition to the method based on wave propagation simulations using orographic maps described in Tabary (2007), long-term rainfall accumulations are used to account for PBB caused by anthropogenic structures and trees.

3) VPR CORRECTION

As described in Tabary (2007), VPR is computed from ratios of hourly rainfall accumulation at different elevations in collocated pixels. Such ratios are used to determine the optimal VPR from a set of predefined VPR models.

4) GAS-INDUCED ATTENUATION CORRECTION

Absorption by atmospheric gases leads to Z_h attenuation (Doviak and Zrnic 1993). The gas-induced attenuation depends on the wavelength and the altitude above sea level. This module estimates the gas attenuation assuming a standard atmosphere and corrects for it.

5) SYNCHRONIZATION

The scans performed during the 5-min cycle are synchronized before combination at the end of the 5-min cycle using the advection field. The advection field is calculated by analyzing the displacement between the current Z_h composite image and the one from the previous cycle using the cross-correlation approach described by Tuttle and Foote (1990).

6) WEIGHTED LINEAR COMBINATION

The best estimation of Z_h on the ground is obtained by combining the measurements performed at different elevations in collocated pixels weighted according to their QI. The value of the maximum QI is kept as a measure of the quality of the multitilt QPE.

7) REFLECTIVITY TO RAINFALL RATE CONVERSION

The Z_h is converted into rainfall rate using the Marshall–Palmer Z–R relationship.

8) 5-MIN RAINFALL ACCUMULATION

The same advection field used in the synchronization is reused to oversample the data to 1-min temporal resolution. The five rainfall fields obtained are added on a pixel basis to get the 5-min rainfall accumulation. Areas of missing data are filled by extrapolating, still with the advection field, the previous 5-min rainfall accumulation.

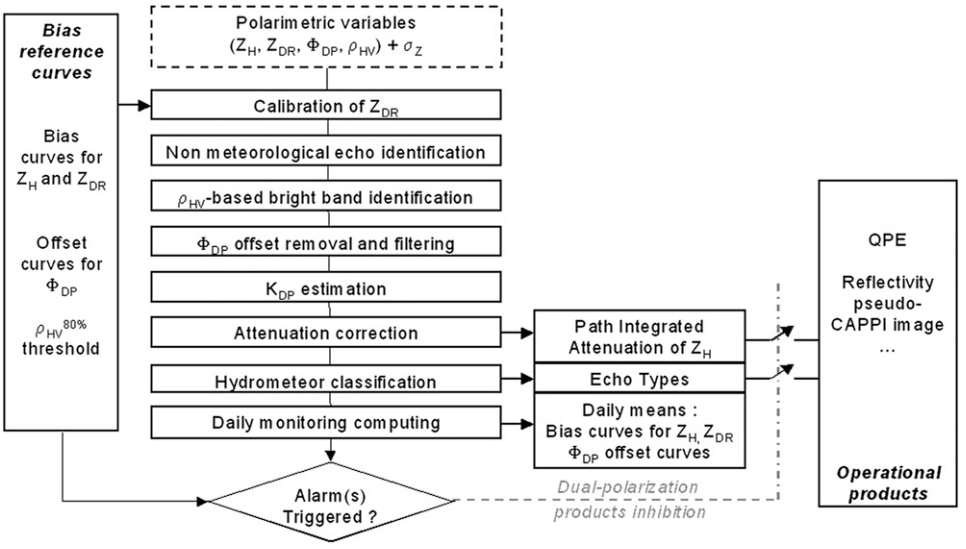

FIG. 2. The polarimetric processing chain.

9) RAIN GAUGE ADJUSTMENT

Despite all the corrections, radar rainfall accumulations still suffer sometimes from nonnegligible biases with respect to rain gauge ground measurements (Fulton et al. 1998; Anagnostou and Krajewski 1999). To minimize those biases, rain gauge data are used to correct the 5-min radar rainfall accumulation field. The adjustment scheme consists of applying one single-bias adjustment factor (AF) to the entire 5-min radar 1-km^2 Cartesian QPE map computed from ratios between rain gauges and collocated radar pixels in the preceding hours. The method to obtain AF is described in detail in Tabary et al. (2011).

b. Polarimetric modules of the operational radar rainfall product

The polarimetric data-processing chain is described in detail in Figueras i Ventura et al. (2012a). The processing chain performs several corrections to the raw polarimetric variables and provides several parameters, notably the echo type and the path-integrated attenuation (PIA) in 1-km^2-resolution Cartesian coordinates, as well as several monitoring parameters.

As can be seen in Fig. 2, the inputs of the polarimetric chain are the polarimetric variables in high-resolution polar coordinates. The variables are oversampled to 240 m $\times$ 0.5° from a typical range resolution of 300 m (2-μs pulse width) and a -3-dB beamwidth between 1.1° and 1.3°. They sequentially undergo a differential reflectivity Z_{dr} calibration; a nonmeteorological echo classification; a brightband identification based on the copolar correlation coefficient ρ_{hv}; a dynamic correction of the system ϕ_{dp} offset and a 25-range-gate moving median filtering to smooth ϕ_{dp} in precipitation gates; the estimation of the specific differential phase K_{dp} using a linear regression of 25 range gates; the attenuation correction of Z_h and Z_{dr}; and the hydrometeor classification by a fuzzy logic algorithm using the polarimetric variables, the brightband altitude and thickness, and the temperature. However, at the moment only two of the outputs are exploited operationally in the rainfall product, the estimated attenuation and the clear-air (CA) echoes identification. The decision to only use a fraction of the potential of polarimetry in a first phase has several motivations. In the first place, since polarimetry is a relatively new concept, there is a need to gradually introduce it to end users and maintenance teams. In the second place, each time a new polarimetric variable is used the downstream processing must be upgraded and time is needed to perform the upgrade.

1) CA ECHOES IDENTIFICATION

The identification of CA echoes is performed by using the echo type determined by the polarimetric chain. The polarimetric chain has a preclassification module that discriminates between CA echoes, GC and precipitation, and noise and missing data. The classification is based on a fuzzy logic algorithm that uses the probability density functions of ρ_{hv}, σ_z, and the Z_{dr} texture of each of the three echo types (Gourley et al. 2007a). In the first version of the polarimetric chain we decided to use only the CA echoes identification and to keep the legacy GC identification schemes of the single polarization chain. The Z_h of the pixels identified as CA echoes by the polarimetric chain is simply set to 0 mm^6 m^{-3}, whereas the QI is kept unchanged.

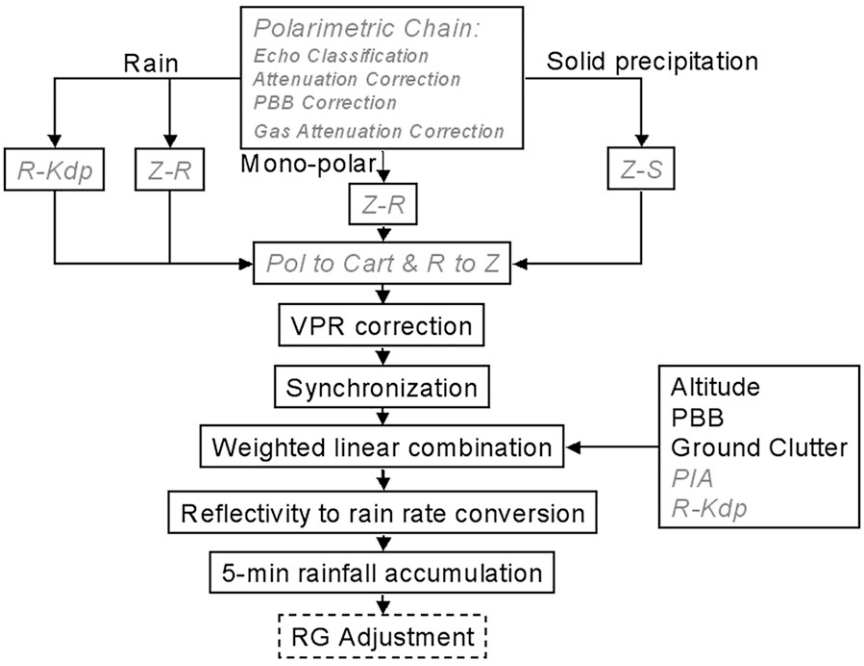

FIG. 3. Flow diagram of version two of the polarimetric radar rainfall product.

2) PRECIPITATION-INDUCED ATTENUATION CORRECTION

The PIA in precipitation is considered to be linearly proportional to ϕ_{dp}. As shown in numerous papers (see, e.g., Bringi et al. 2001; Tabary et al. 2009; Rico-Ramirez 2012) the coefficient of proportionality γ_h varies according to the wavelength, temperature, hydrometeor shape, hydrometeor size distribution, and the presence of large hydrometeors causing Mie scattering. However, for the sake of simplicity and because of the difficulties in determining all the factors involved, in this first version a single value for each frequency is used in all precipitation types. The coefficient at C band was determined empirically using data from the Trappes radar (see Gourley et al. 2007b) to be 0.08 dB $(°)^{-1}$. The S-band coefficient was taken from Bringi and Chandrasekar (2001): 0.04 dB $(°)^{-1}$. The coefficient at X band was extracted from joint S-band–X-band measurements (see Tabary et al. 2008): 0.28 dB $(°)^{-1}$.

The aforementioned polarimetric modules are placed between the clutter identification and the PBB correction of the single polarization chain. The rest of the processing chain is left unchanged.

3. Second version of the polarimetric radar rainfall product

The new polarimetric radar product aims at improving the performance in three major aspects: better echo classification, better precipitation estimation, and a lower detectability threshold. It also paves the way for higher spatial resolution products (250 m) by performing most of the data processing in high-resolution (0.5° × 240 m) polar coordinates and for the retrieval of the vertical profile of equivalent liquid water precipitation rates by treating each hydrometeor type separately. As can be seen in Fig. 3, the echo classification is now fully performed by the polarimetric chain. The necessary corrections on Z_h at each individual scan are also performed by the polarimetric chain with the aim of having the best quality polarimetric variables entering into the hydrometeor classification. Based on that, several modules have been added to the polarimetric chain.

The first module treats extra noise filtering. The noise filtering in the previous products is performed by finding the minimum received power per scan and adding a certain margin to account for the noise standard deviation. It has been recognized that emission from ground clutter results in an increase in the noise floor, which is spatially dependent. Therefore the new noise filter finds the minimum received power at far range per ray.

The second module is the PBB Z_h correction. The procedure is exactly the same as previously described. The only difference is that the correction is performed in high-resolution polar coordinates instead of Cartesian coordinates.

The third module is the gas-induced attenuation correction. Again, the difference is that the correction is performed in polar coordinates.

The fourth module is for detection of GC using a static GC map. Polarimetric variables may not be usable either because of hardware or data transmission problems or because the signal-to-noise ratio (SNR) is too low. A very restrictive threshold of 15-dB SNR has been set on the use of polarimetry to ensure high-quality polarimetric data. In such case the GC detection is performed using a threshold on σ_z. Areas of frequent GC have a more restrictive threshold. The ground cluttered areas have been determined a priori by observing the median values of Z_h over an entire nonprecipitating day.

In the QPE module, the rainfall rate is estimated differently according to the echo type. Solid precipitation (snow, ice, etc.) is estimated using a Z–R relationship where Z_h has been attenuation corrected. In areas where polarimetry was not available (e.g., SNR < 15 dB), Z_h is also converted into rainfall rate using a Z–R relationship. For the quantification of rain a hybrid estimator is used. If K_{dp} is above a certain threshold a K_{dp}–R relationship of the form

$$R = a\left(\frac{K_{\mathrm{dp}}}{f}\right)^{b}, \tag{1}$$

where f is the central frequency in gigahertz, is applied; otherwise a Z–R relationship is used. Notice that Z_{dr} is not used in the QPE because its current stability was considered insufficient (see Figueras i Ventura et al. 2012a). The threshold is based on the K_{dp} value because it is insensitive to attenuation, calibration errors, and PBB. At the moment, the Z–R relationship used for all the estimators is the Marshall–Palmer. Below the threshold level, K_{dp} is considered to be too noisy to be used. The K_{dp}–R relationship used at S and C bands is derived from the Beard and Chuang (1987) drop shape (i.e., $a = 129$ and $b = 0.85$) [which provided the best performance in the study by Figueras i Ventura et al. (2012a)] and is used for K_{dp} above 1° km^{-1}. Studies at X band by Kabeche et al. (2012) found that the Brandes et al. (2002) ($a = 132.44$ and $b = 0.791$) K_{dp}–R relationship is more suitable at X band and that above 0.5° km^{-1} K_{dp} is sufficiently noise-free to be usable.

The next module added was polar to Cartesian coordinate conversion. The legacy processing is performed on Z_h in Cartesian coordinates. The rainfall-rate output of the polarimetric chain is converted into 1-km^2 Cartesian coordinates using the nearest-neighbor approach and back to Z_h using the inverse Marshall–Palmer Z–R relationship.

The final module added addresses the reflectivity detectability threshold. It is a common, yet sometimes wrong, assumption to consider that pixels at noise level correspond to valid, no-rain areas. In the presence of attenuation, and especially at short wavelengths, this is clearly a wrong assumption. The precipitation detectability depends on the sensitivity of the radar but also on the presence of PBB, on the level of GC, and the attenuation suffered by the signal. It is therefore a space–time-varying parameter. The precipitation-induced attenuation in particular increases with the radar frequency. It is therefore important to inform the user of the minimum rainfall rate detectable since, when severe convective cells are present, precipitation farther away may not be detectable by the radar. It is also an important parameter to determine up to which distance from the radar low Z_h phenomena like fog can be detected. Furthermore, this is essential information when performing multiradar combination (Maesaka et al. 2011).

The new radar product provides information of Z_h detectability together with the 5-min rainfall accumulation. The module estimates the detectability of each scan in the 5-min cycle by taking into account the noise level, the PBB, the gas- and precipitation-induced attenuation, and the Z_h level of the detected ground clutter. The detectability of precipitation on the ground is then considered to be the minimum detectable Z_h of all collocated measurements at the vertical below 10 km.

Figure 4 provides an example of the variability of the detectability threshold. It corresponds to a precipitation event that was observed by the Mont Maurel X-band radar on 4 September 2010. At 0505 UTC (Fig. 4c), when no significant precipitation is present (see Fig. 4a), the detectability is homogeneous, setting aside areas of GC close to the radar and the effect of PBB in some sectors. At 0640 UTC, there are several active convective cells in the area (see Fig. 4b). In sectors farther away from the cells, the detectability increases, reaching levels up to 30 dBZ (i.e., $\sim$3 mm h^{-1}).

4. Old and new quality indexes

The QI is used as an indicator of the confidence on the measurement at pixel level. The QI at pixel level determines the weight that the measurement has in the multitilt combination. The maximum of the QIs in a multitilt combination is a qualitative indicator of the uncertainty of the measurement on the ground. It is used to determine the pixel weight when performing the multiple radar composite.

The QI of the operational radar rainfall product depends on the echo classification, the estimated percentage of beam blockage, and the altitude of the measurement. The dependency is linked to the uncertainty in the corrections performed. If the PBB or VPR corrections were perfect they would not impact the QI. This dependency is expressed as follows:

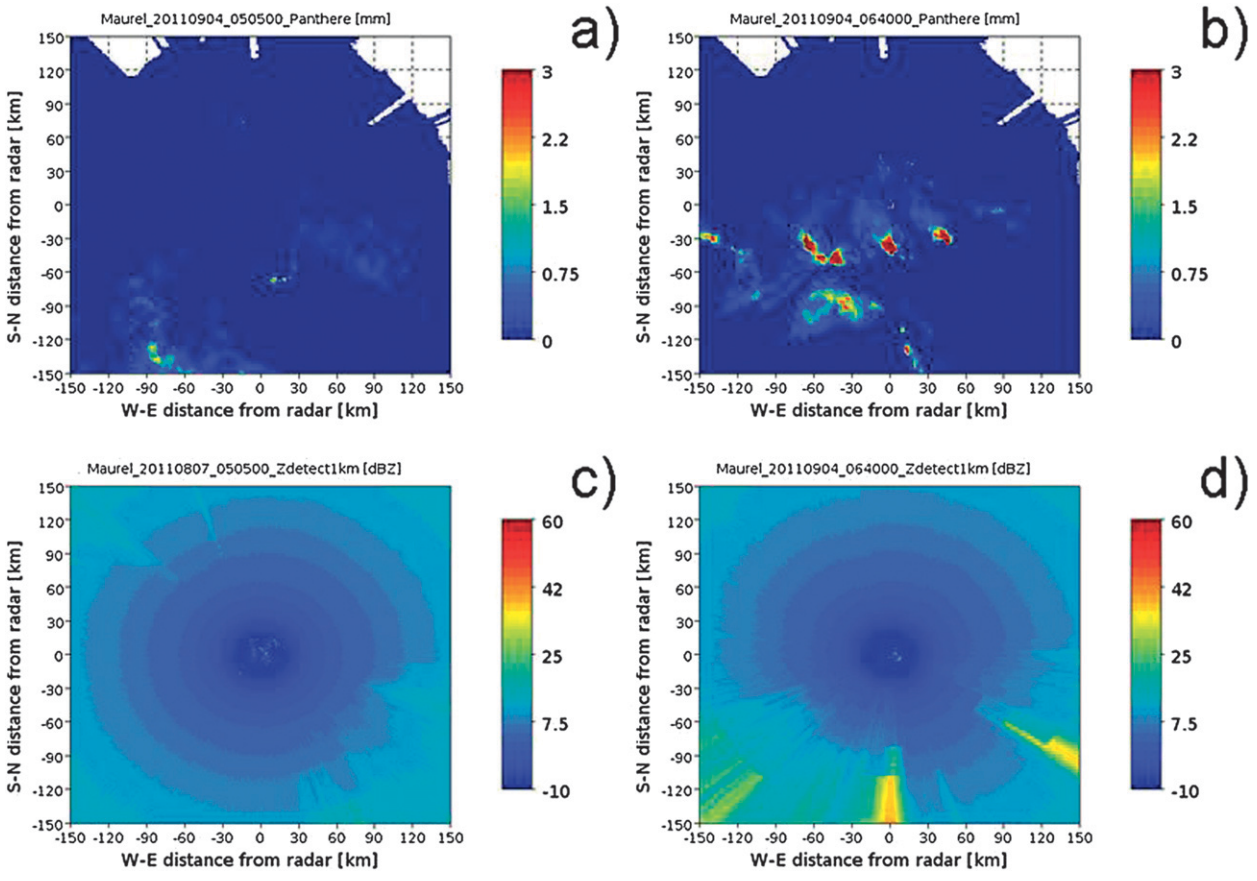

FIG. 4. Example of Z_h detectability at two different instants. The event occurred in Mont Maurel on 4 Sep 2011. The images correspond to 5-min rainfall accumulation at (a) 0505 UTC and (b) 0640 UTC and Z_h detectability at (c) 0505 UTC and (d) 0640 UTC.

$$\omega(x,y) = \omega_{\mathrm{GC}}(x,y)\omega_{\mathrm{PBB}}(x,y)\omega_h(x,y). \qquad (2)$$

The ω_{GC} is 1 when the pixel is classified as precipitation or its Z_h is below 8 dBZ and 0 otherwise.

The dependence with the percentage of PBB is considered linear and can be expressed as follows:

$$\omega_{\mathrm{PBB}}(x,y) = \begin{cases} 1 - \dfrac{\mathrm{PBB}(x,y)}{100} & \mathrm{PBB}(x,y) < 70 \\ 0 & \mathrm{PBB}(x,y) \geq 70 \end{cases}. \qquad (3)$$

The dependence with height above the ground is considered exponential of the form

$$\omega_h(x,y) = \begin{cases} e^{[-h(x,y)-h_G(x,y)/h_o]} & h(x,y) - h_G(x,y) < 10\,\mathrm{km} \\ 0 & h(x,y) - h_G(x,y) \geq 10\,\mathrm{km} \end{cases}, \qquad (4)$$

where h_G is the altitude of the ground above sea level, h is the altitude of the measurement above sea level, and $h_o = 0.5\,\mathrm{km}$.

Figure 5c shows an example of QI. It decreases with distance as a consequence of the increased elevation of the radar beam and with PBB. Notice the low QI spots close to the radar, which correspond to areas of clutter where a higher tilt is predominant in the composite.

The second version of the polarimetric radar rainfall product adds the dependence on PIA:

$$\omega(x,y) = \omega_{\mathrm{GC}}(x,y)\omega_{\mathrm{PBB}}(x,y)\omega_h(x,y)\omega_{\mathrm{PIA}}(x,y), \qquad (5)$$

where

$$\omega_{\mathrm{PIA}}(x,y) \begin{cases} 1 & R(K_{dp}) \\ 1 - \dfrac{\mathrm{PIA}(x,y)}{\mathrm{PIA}_O} & \mathrm{PIA}(x,y) < \mathrm{PIA}_O \\ 0 & \mathrm{PIA}(x,y) \geq \mathrm{PIA}_O \end{cases}. \qquad (6)$$

The weight is kept to 1 when rainfall rate is estimated using K_{dp} since it is insensitive to precipitation attenuation.

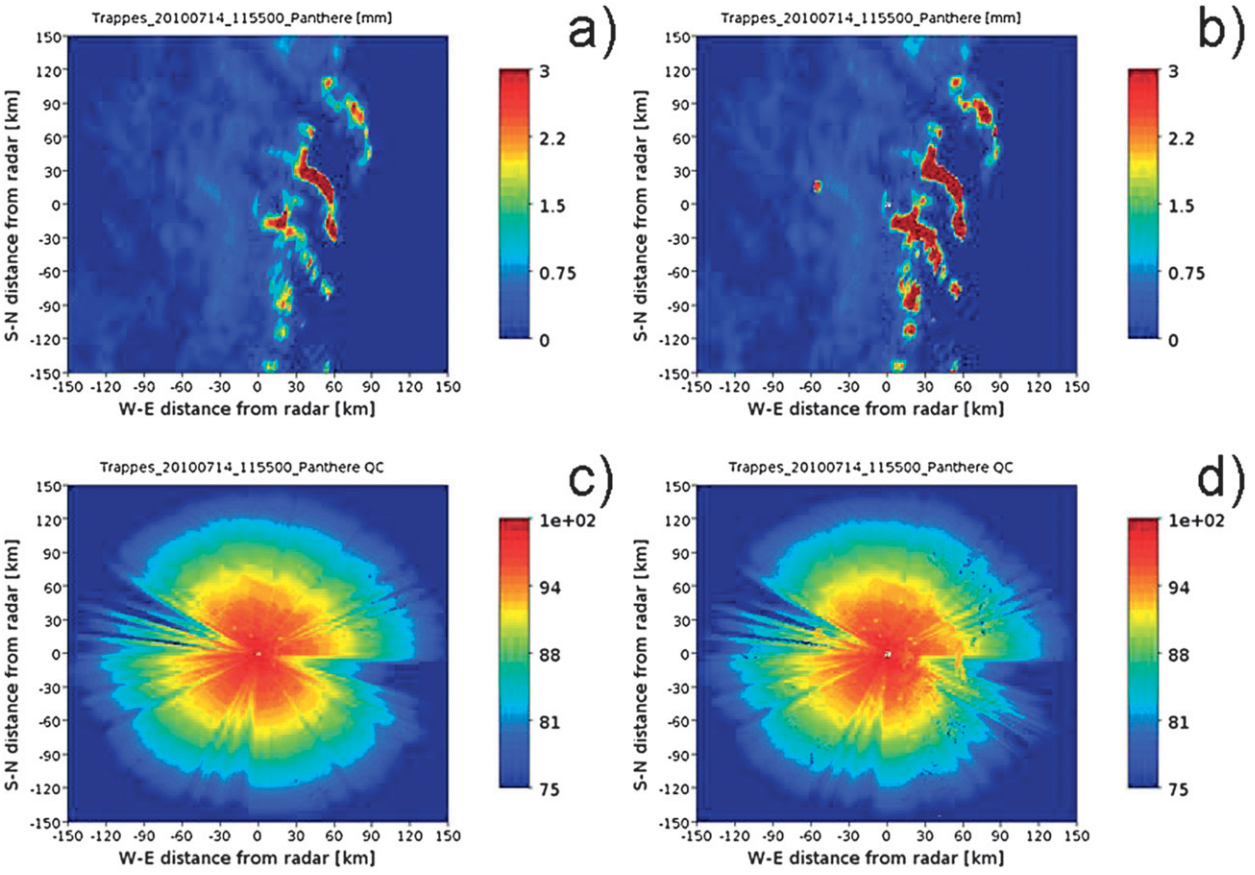

FIG. 5. Example of (a),(b) 5-min rainfall accumulation and (c),(d) associated QI. The event occurred in Trappes at 1155 UTC 14 Jul 2010. (left) Version 1 of the polarimetric radar rainfall product, and (right) version 2.

The quantity PIA_O is set to 40 dB. For the same reason, ω_{PBB} is modified as follows:

$$\omega_{\mathrm{PBB}}(x,y)\begin{cases}1 & R(K_{\mathrm{dp}})\\ 1-\dfrac{\mathrm{PBB}(x,y)}{100} & \mathrm{PBB}(x,y)<70\\ 0 & \mathrm{PBB}(x,y)\geq 70\end{cases}. \quad (7)$$

Finally, ω_{GC} is kept to 0 if GC is identified, regardless of the Z_h value.

Admittedly, the formulation of the weight dependency with respect to PIA is at the moment rather arbitrary. Studies at X band (Tabary et al. 2008) showed that the PIA standard deviation is linearly constant in relative terms, and therefore the error committed in its estimation is linearly increasing. The rather high PIA_O threshold is a trade-off between the need to reflect the increase of uncertainty in the measurement due to PIA while at the same time allowing the use of highly attenuated data at X band. A more specific study on the optimal formulation of the PIA dependency at different wave lengths is required but is out of the scope of this paper. However, it should be noticed that the most significant impact of the PIA weight is in the multiradar composite.

The quality index used in the multitilt combination decreases very fast with altitude. It is for this reason that in the multiradar combination it is not used directly but is finally expressed as

$$\Omega=\begin{cases}0 & \omega^{h_0}<e^{-10}\\ 100\left[1+0.1\ln\left(\omega^{h_0}\right)\right] & \omega^{h_0}\geq e^{-10}\end{cases}. \quad (8)$$

Figure 5d shows an example of the new QI for the same event as the one shown in Fig. 5c. Comparing the two images, the difference in QI can be appreciated. In Fig. 5d there are more spots close to the radar because the GC identification criteria is more strict. The use of K_{dp} results in a higher QI in areas of PBB (see the area west of the radar). On the other hand, in areas with large attenuation, where Z_h is used (just behind the convective cells) to obtain the rainfall rate, the QI is lower.

5. Products evaluation

a. Data selection and evaluation methodology

The three radar rainfall products—the single polarization (hereinafter CONV), the first version of the polarimetric chain (hereinafter DBP1), and the second version of the polarimetric chain (hereinafter DBP2)—have been evaluated offline using several precipitation episodes. The final Météo France product is adjusted using rain gauges, but, to strictly evaluate the performance of the processing chain, data before the rain gauge adjustment have also been analyzed.

The 5-min rainfall accumulation obtained by CONV and DBP1 is hourly accumulated using a very strict criterion whereby if one of the 12 pixels in the time series is not valid within the hour the hourly accumulation is set to ''data not available.'' Unlike the other products, DBP2 invalidates pixels containing GC with very low Z_h. For this reason a slightly different criterion has been taken to validate the hourly accumulation. In that case, if a maximum of two pixels are invalid but they have a Z_h threshold below 5 dBZ, the invalid pixels are set to have a 0-mm rainfall accumulation and the hourly accumulation is considered valid.

The hourly rainfall accumulations are compared against hourly rain gauges. The Météo France rain gauge network consists of tipping-bucket gauges with a bucket resolution of 0.2 mm; that is, the minimum hourly rainfall accumulation that can be measured is 0.2 mm. All rain gauge data are routinely quality controlled as described in Figueras i Ventura et al. (2012a). The radar–rain gauge comparison is done by matching each rain gauge with the corresponding radar pixel. It is important to notice that the comparison between rain gauges and radar data is subject to additional uncertainties. In the first place there is the uncertainty in the rain gauge measurement, which is inversely proportional to the rainfall rate (Ciach 2003). Second, the fact that the rain gauge is a point measurement whereas radar measurements are areal introduces a representativeness error that is proportional to the spatial variance of the rainfall field (Emmanuel et al. 2012). Despite these extra sources of uncertainty, the comparison with rain gauges remains the best tool to objectively assess the performance of a QPE algorithm.

The quality of the algorithms is evaluated using the normalized bias (NB) between the rain gauge and the radar rainfall accumulation defined as

$$\mathrm{NB} = \frac{\langle R \rangle}{\langle G \rangle} - 1, \tag{9}$$

where $\langle\rangle$ denotes the average, the correlation (corr)

$$\mathrm{corr} = \frac{\sum_{\forall i} (G_i - \langle G \rangle)(R_i - \langle R \rangle)}{\sqrt{\sum_{\forall i} (G_i - \langle G \rangle)^2} \sqrt{\sum_{\forall i} (R_i - \langle R \rangle)^2}}, \tag{10}$$

the root-mean-square error (RMSE)

$$\mathrm{RMSE} = \sqrt{\frac{\sum_{\forall i} (R_i - G_i)^2}{n}}, \tag{11}$$

and the Nash–Sutcliffe model efficiency coefficient (Nash)

$$\mathrm{Nash} = 1 - \frac{\sum_{\forall i} (R_i - G_i)^2}{\sum_{\forall i} (G_i - \langle G \rangle)^2}. \tag{12}$$

In addition, the dispersion defined as the percentage of radar–rain gauge ratios outside the interval 0.8–1.25 has also been calculated.

The present study is focused on a warm period, where the benefits of the polarimetric QPE algorithms are more relevant because for the moment they are only applied in rain and the range at which the lowest tilt crosses the bright band is larger during that period. The selection of events is performed objectively using three criteria. First, the daily average ground temperature close to the radar must be high enough so that the upper edge or the radar −3-dB beam was below the freezing-level height at 60 km. A standard atmosphere temperature decrease of −6° km is used to estimate the altitude of the freezing-level height. Second, a significant amount of rain must be present in the vicinity of the radar. The amount of rain is determined by calculating the average daily rainfall accumulation of all the rain gauges within a 60-km-radius area. Events with an average rainfall accumulation higher than 5 mm are considered. Finally, all the selected events should have been observed using the same scan strategy.

For S and C band, data from the year 2010 are analyzed. At C band, four different radars out of the nine present that year from different regions are used. They are considered to be representative of the entire radar network. For the evaluation at S band, events observed by the Nimes radar, the sole S-band radar in the network in 2010, are analyzed. The X-band radar is analyzed using data from Maurel, which has a raw data processor similar to the one used by the radars in the operational network (Parent du Chatelet et al. 2001). Data from Maurel are available since the second half of 2011. Table 1 lists the radar–event couples that result from the selection.

TABLE 1. Events used for the evaluation.

Frequency	Radar	Date
S band	Nimes	6, 7 Sep; 9, 10 Jul 2010
C band	Avesnes	12, 14 Jul; 15, 16, 26 Aug 2010
	Blaisy	21, 22 Jul; 15, 16, 23, 27 Aug; 7 Sep 2010
	Montancy	28, 29 Jul; 2, 5, 12, 14, 15, 16, 24, 27 Aug 2010
	Trappes	3, 12, 14 Jul; 15 Aug 2010
X band	Maurel	27 Jul; 7 Aug; 4 Sep; 4 Nov 2011

b. General results

The results are stratified according to three thresholds on the rain gauge hourly accumulations: ≥ 0.2 mm [all rainfall accumulations (AR)], ≥ 1 mm [moderate and high hourly accumulations (MR)], and ≥ 5 mm [intense hourly accumulations (IR)]. The results are obtained in the area 60 km around the radar, which has the best hydrological visibility. The number of rain gauges available in this area varies from 20 to 40 depending on the radar location. Table 2 summarizes the scores obtained by each product at each frequency.

1) RESULTS AT S BAND

The global results obtained by each rainfall product are represented in Fig. 6. The evaluation is performed before and after the rain gauge adjustment to clearly determine the impact of the different ways to process the data on the results. As can be seen in Fig. 6a, the CONV product slightly underestimates precipitation (NB = −0.13 for AR). The underestimation is more pronounced at IR (NB = −0.27). As shown in Fig. 6b, the rain gauge adjustment is able to globally correct for such underestimation but intense precipitations remain underestimated (NB = −0.13). The use of the DBP1, which basically corrects for precipitation-induced attenuation results in an improvement of NB and corr as shown in Fig. 6c. Such improvement is even more relevant at IR (NB reduced from −0.27 to −0.18) as shown in Fig. 6d. The rain gauge adjustment is less dramatically beneficial for the DBP1 and the final results are comparable with those obtained by the CONV product. Nevertheless, minor improvements with respect to CONVadj should be pointed out. As represented in Fig. 6e, DBP2 obtains the best score in all categories. Particularly outstanding is the NB at IR, which is reduced by one-third compared to that of CONV. The application of the rain gauge adjustment, though, does not significantly improve the results, as shown in Fig. 6f.

2) RESULTS AT C BAND

The global results at C band are represented in Fig. 7. As can be seen in Fig. 7a, the radar largely underestimates precipitation (−0.32 for AR and up to −0.47 for IR). Corr is rather poor as well for IR. This large underestimation can be attributed to precipitation-induced and radome-induced attenuation, but miscalibration of Z_h should not be discarded. The rain gauge adjustment significantly reduces NB (down to −0.10 for AR and −0.28 for IR) and it has a positive impact also on corr (and increase of 0.04 in the score; see Fig. 7b). The positive impact of the attenuation correction of DBP1 is readily visible in Fig. 7c. NB for AR is reduced to −0.25, but the most positive impact is, as expected, in IR, where

TABLE 2. Summary of the results.

		Precipitation ≥ 0.2 mm				Precipitation ≥ 1 mm				Precipitation ≥ 5 mm			
Band	Product	NP	NB	corr	RMSE	NP	NB	corr	RMSE	NP	NB	corr	RMSE
S	CONV	1533	−0.13	0.88	3.96	1028	−0.17	0.88	4.79	175	−0.27	0.82	11.23
	DBP1	1533	−0.09	0.90	3.54	1028	−0.11	0.90	4.27	175	−0.18	0.84	9.91
	DBP2	1519	−0.04	0.92	3.08	1017	−0.06	0.92	3.72	173	−0.09	0.88	8.46
	CONVAdj	1533	−0.00	0.88	3.71	1028	−0.03	0.88	4.46	175	−0.13	0.82	10.16
	DBP1Adj	1533	−0.01	0.90	3.51	1028	−0.03	0.89	4.22	175	−0.11	0.84	9.64
	DBP2Adj	1519	−0.01	0.92	3.10	1017	−0.03	0.92	3.73	173	−0.09	0.88	8.38
C	CONV	7162	−0.32	0.78	1.92	4156	−0.36	0.73	2.49	626	−0.47	0.54	5.78
	DBP1	7162	−0.25	0.83	1.64	4156	−0.28	0.80	2.11	626	−0.37	0.70	4.58
	DBP2	7134	−0.19	0.85	1.59	4151	−0.22	0.83	2.01	624	−0.19	0.79	4.18
	CONVAdj	7162	−0.10	0.82	1.61	4156	−0.14	0.77	2.05	626	−0.28	0.58	4.63
	DBP1Adj	7162	−0.10	0.85	1.45	4156	−0.13	0.83	1.83	626	−0.24	0.71	3.98
	DBP2Adj	7134	−0.09	0.87	1.39	4151	−0.12	0.85	1.73	624	−0.16	0.79	3.57
X	CONV	1485	−0.62	0.62	3.25	946	−0.66	0.56	4.06	237	−0.74	0.52	7.47
	DBP1	1485	−0.41	0.71	2.61	946	−0.44	0.67	3.22	237	−0.51	0.63	5.73
	DBP2	1485	−0.19	0.77	2.26	946	−0.22	0.73	2.75	237	−0.28	0.70	4.39
	CONVAdj	1485	−0.29	0.63	2.75	946	−0.34	0.56	3.34	237	−0.49	0.52	5.89
	DBP1Adj	1485	−0.07	0.72	2.56	946	−0.12	0.67	3.06	237	−0.22	0.62	4.91
	DBP2Adj	1485	−0.03	0.78	2.39	946	−0.07	0.74	2.89	237	−0.11	0.70	4.30

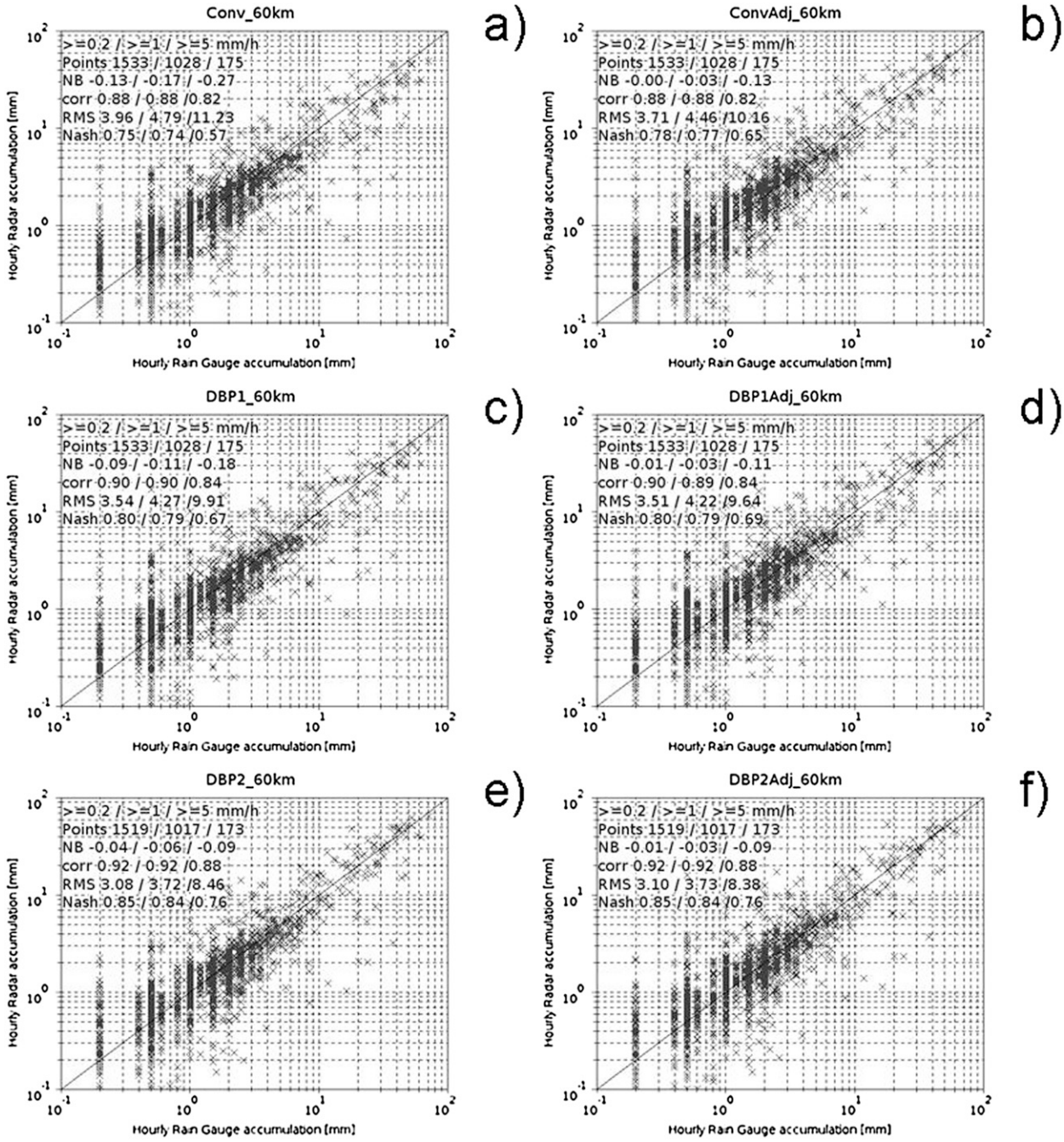

FIG. 6. Scatterplot of the hourly precipitation accumulation of rain gauge data with respect to S-band radar data: (a) CONV, (b) CONVAdj, (c) DBP1, (d) DBP1Adj, (e) DBP2, and (f) DBP2Adj.

both NB and corr are greatly improved (NB down to −0.34 and corr up to 0.70). With the rain gauge adjustment a similar score in terms of NB to CONVAdj is obtained but corr is further improved (see Fig. 7d). Again, the best score is obtained by DBP2, with the most noticeable improvement on the IR (NB = −0.19 and corr up to 0.79, see Fig. 7e). The improvement due to rain gauge adjustment is less significant, particularly that of IR (see Fig. 7f).

3) RESULTS AT X BAND

The global results obtained at X band are represented in Fig. 8. The radar of Maurel is situated in a mountainous environment. The estimation of surface precipitation in

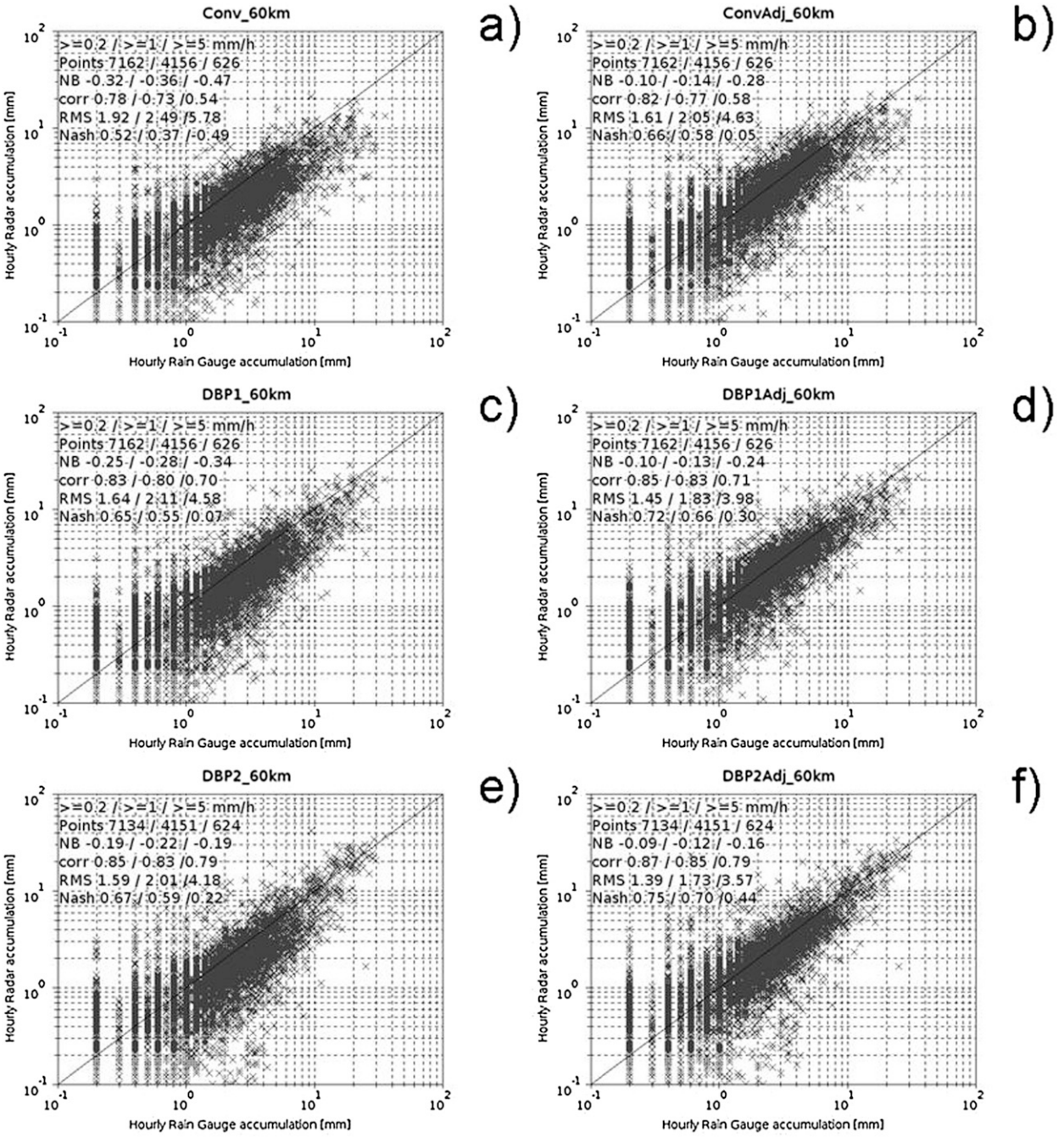

FIG. 7. As in Fig. 6, but with respect to C-band radar data.

such an environment is rendered more difficult because of PBB and the fact that measurements are performed high above the ground. In addition, rain gauges tend to be placed in valleys; orographic enhancement effects not measurable by the radar should not be discarded in such conditions. This is the likely cause for the extremely low corr exhibited by the CONV method shown in Fig. 8a. Part of the very large negative NB of the measurement can be attributed to radar miscalibration. In a separate study, a radar-to-radar comparison in collocated pixels was performed between the radar at Mont Maurel and that at Mont-Vial (Frasier et al. 2012). The study concluded that the Mont Maurel radar was underestimating Z_h by 2 dB with respect to the Mont-Vial radar. Another cause for the underestimation of precipitation is wet radome attenuation, the effect of which is more significant

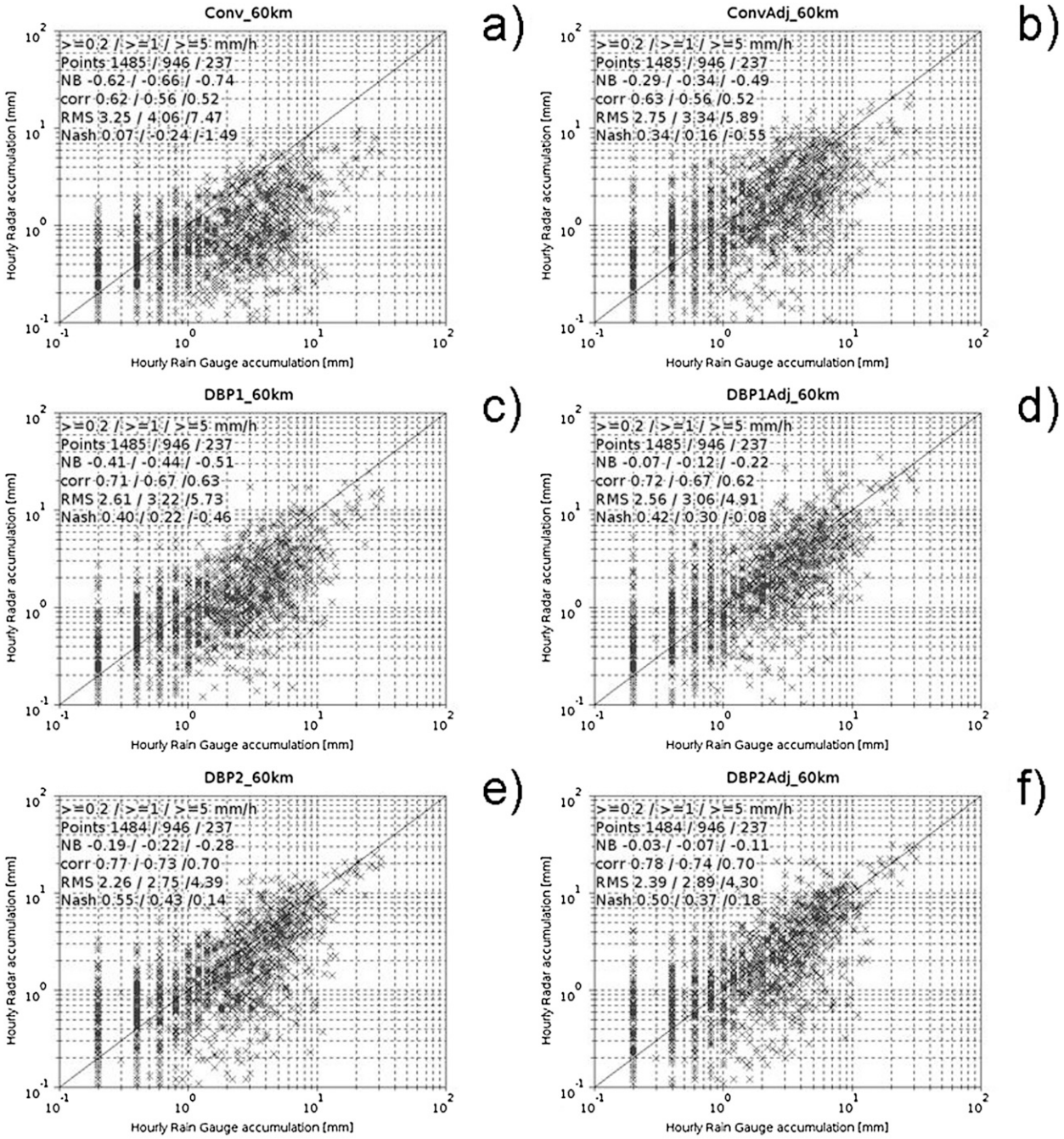

FIG. 8. As in Fig. 6, but with respect to X-band radar data.

at X band that at a lower frequency. Again, the adjustment using rain gauges significantly reduces NB although it fails to improve the corr (see Fig. 8b). As shown in Fig. 8c, the attenuation correction of DBP1 results in a reduction of roughly 0.2 in NB and an improvement of 0.1 in corr. The use of the rain gauge adjustment improves the NB by roughly 0.2 with respect to CONVAdj (see Fig. 8d). The best results by far are obtained by DBP2 (see Fig. 8e). The use of K_{dp}, which is insensitive to wet radome attenuation and PBB, largely reduces NB and it significantly increases corr. The rain gauge adjustment further reduces NB (see Fig. 8f). The NB obtained by DBP2Adj is comparable to that obtained at the other frequency bands.

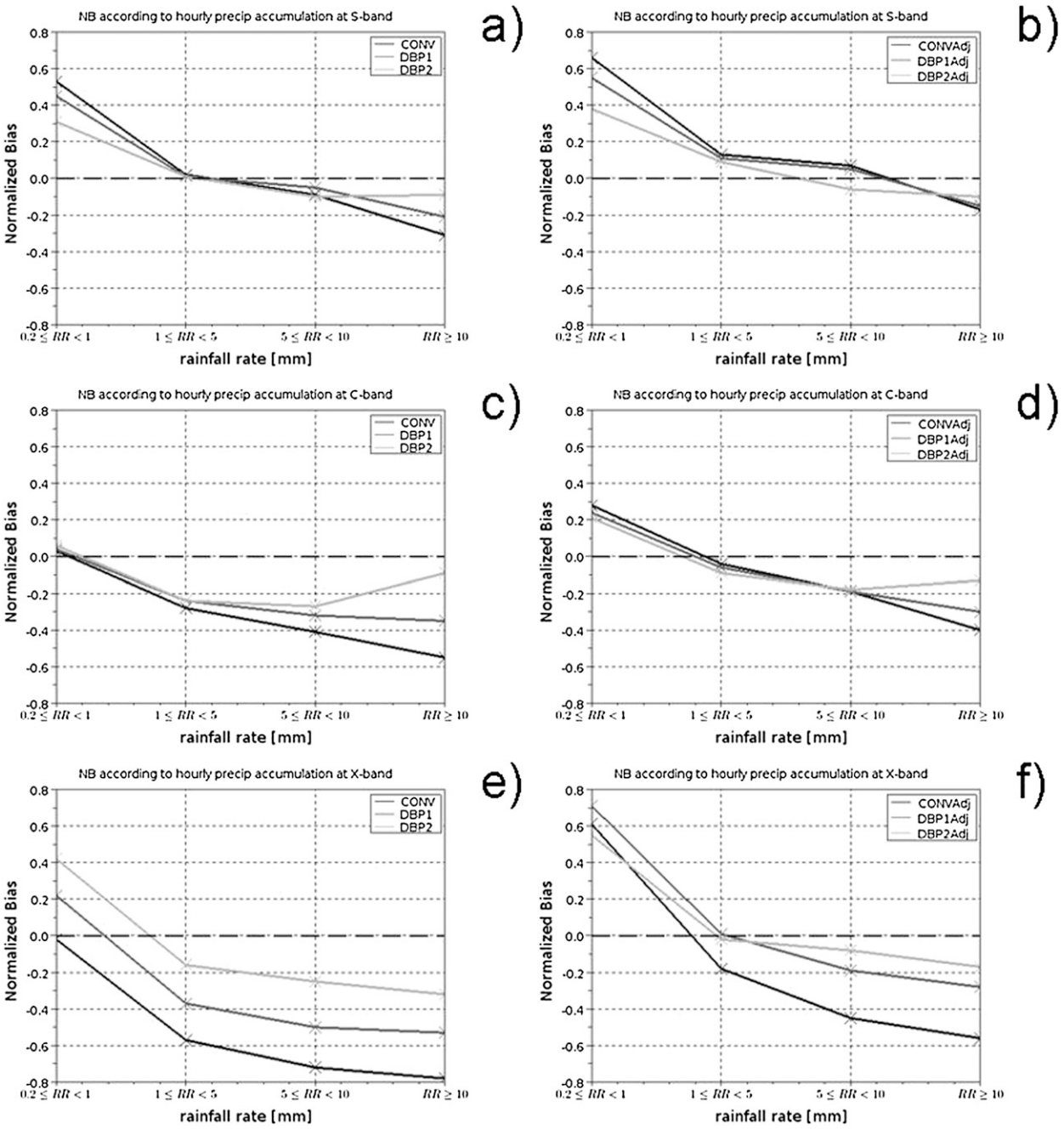

FIG. 9. The NB of the different products stratified by hourly rainfall accumulation (a) at S band, (b) at S band with rain gauge adjustment, (c) at C band, (d) at C band with rain gauge adjustment, (e) at X band, and (f) at X band with rain gauge adjustment.

c. Stratification by rainfall accumulation

Figures 9 and 10 show NB (Fig. 9) and the dispersion (Fig. 10) obtained by each product at each frequency band stratified by hourly rain gauge rainfall accumulation. As can be seen, the NB of the CONV product shows the same trend at all frequency bands with a large overestimation of the weak precipitation and a large underestimation of intense precipitation. The large offset on weak precipitation may be due to the larger relative contribution of noise and collocated clutter on Z_h. Currently, the noise is not subtracted from the signal. The dispersion, on the other hand, is higher for weak precipitation, gets better at moderate rainfall accumulations, and increases again for more intense precipitation. This is the trend at S and C band (see Figs. 10a,c). At X band

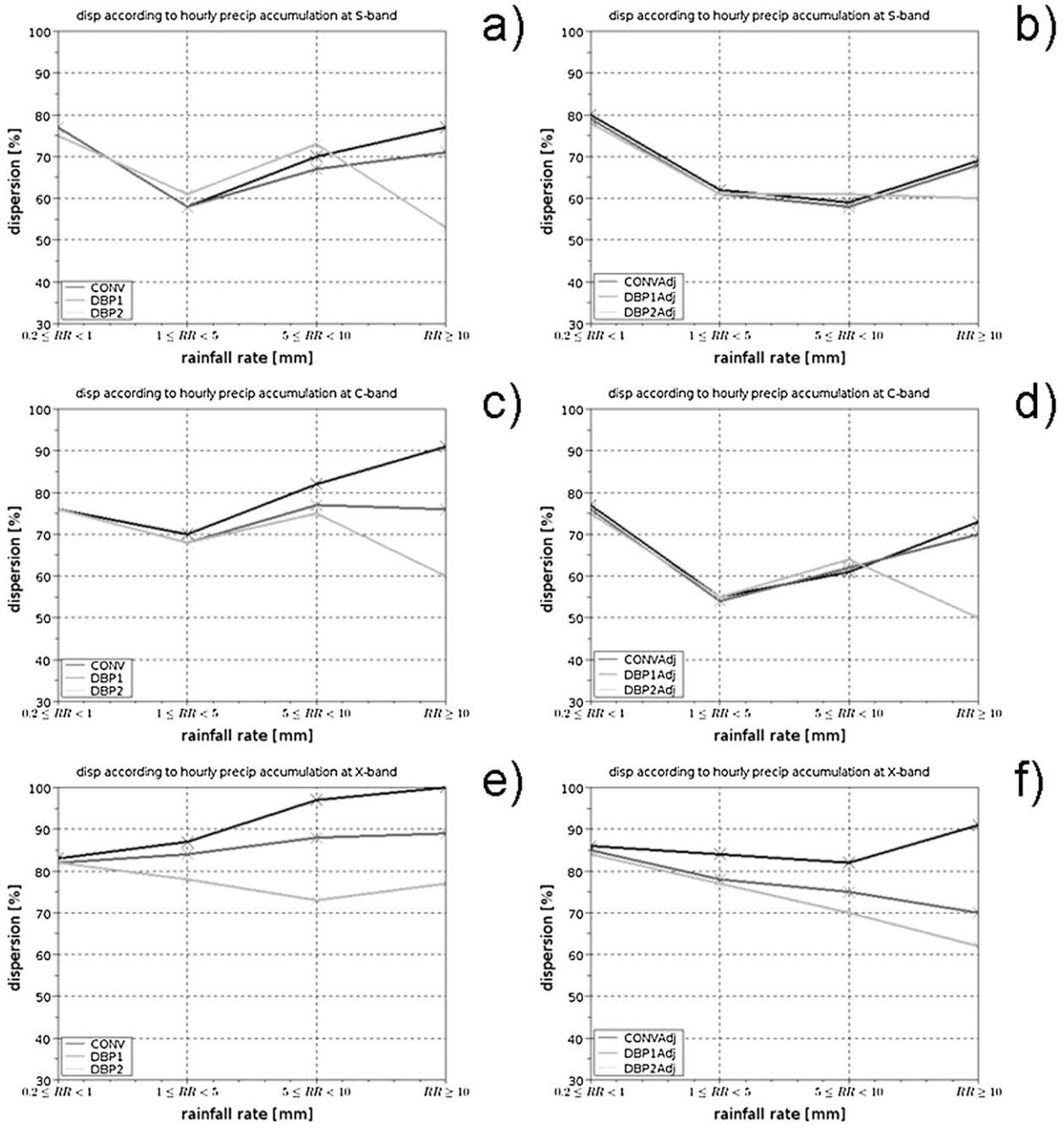

FIG. 10. As in Fig. 9, but for the dispersion of the different products.

(Fig. 10e), because of the very large NB, the dispersion is higher and the results are worst at moderate rainfall accumulations than at weak precipitation.

The rain gauge adjustment corrects for the offset of the NB curve but does not have a significant impact on its shape. At S and C band, the rain gauge adjustment results in NB close to zero for moderate precipitation (1–5 mm; see Figs. 9b,d). This type of rain is the most common and consequently the one with the highest weight in setting the adjustment coefficient. At S band, NB becomes positive for all rainfall accumulation classes except those above 10 mm (see Fig. 9b). At X band (see Fig. 9f), the rain gauge adjustment fails to compensate the very large NB. The impact of the rain gauge adjustment is much more noticeable looking at the dispersion. At S band (Fig. 10b), the improvement is visible at rainfall

accumulation above 5 mm. At C band (Fig. 10d), the improvement is more pronounced and it is already noticeable above 1-mm rainfall accumulations. At X band (see Fig. 10f), the improvement is also noticeable although the values remain high.

As expected, the impact of the attenuation correction performed by DBP1 is more visible at larger rainfall accumulations and higher-frequency bands. It should be noticed that while at C and X band (Figs. 9d,f) the correction results in a similar NB for all precipitations above 5 mm, at S band (Fig. 9b) NB after the correction is still larger for rainfall rates above 10 mm. That suggests an underestimation of the attenuation at S band. The larger NB observed by CONV in the weakest precipitation compared to DBP1 is attributed to the better filtering of clear air, the impact of which is larger at lower-frequency bands. The effect on the dispersion is an improvement, particularly for larger rainfall accumulations.

The application of the rain gauge adjustment results in NB scores similar to those obtained by CONVAdj at S and C band (see Figs. 9b,d). The larger rainfall accumulations have somewhat a smaller (less negative) NB, in particular at C band, while the weakest rainfall accumulations have a smaller (less positive) NB. This is due to the fact that the adjustment coefficient is smaller since the NB at moderate precipitation accumulations is smaller when attenuation is corrected. At X band (see Fig. 9f), the rain gauge adjustment succeeds in obtaining a NB close to 0 for moderate rainfall accumulation, at the expense of a large increase in NB for small rainfall accumulations. The dispersion at S and C bands (Figs. 10b,d) using DBP1Adj has very similar values. Only at X band (Fig. 10f) does the use of DBP1Adj result in a significantly better score.

DBP2 provides the best overall results at all frequency bands and all rainfall accumulation categories, except for the smaller rainfall accumulation at X band. At S and C bands the impact of the R–K_{dp} estimator is visible for hourly rainfall accumulations larger than 5 mm (see Figs. 9a,c). At X band, the effect is visible even at small rainfall accumulations because this frequency band suffers from a much larger precipitation-induced attenuation and the K_{dp} threshold is set to 0.5° instead of 1.0° (see Fig. 9e). Somewhat surprising is the larger negative NB with respect to DBP1 for rainfall accumulations between 5 and 10 mm at S band. It is also noteworthy that at C band, DBP2 has a smaller NB for rainfall accumulations larger than 10 mm than that of accumulations between 5 and 10 mm. The shape of the NB curve above 1 mm of DBP1 is rather flat, suggesting that the attenuation is indeed well corrected. The combination of these results suggests that most of the C-band radars in the network tend to underestimate Z_h. The dispersion of DBP2 is rather similar to the other processing modes except at large rainfall accumulation where it is remarkably better, getting smaller than 60% at S and C band (see Figs. 10a,c).

The fact that moderate precipitation accumulations have a smaller NB in DBP2 with respect to the other products results in a smaller rain gauge adjustment coefficient. Consequently, the large positive NB for small precipitation accumulations in the other rain gauge–adjusted products is reduced while NB at the largest rainfall accumulations is much closer to 0 (see Figs. 9b,d,f). It is noticeable the fact that NB for rainfall accumulations above 10 mm is increased with respect to DBP2 at C band (see Fig. 9b). The adjustment by rain gauges gets the dispersion score very close to that of CONVAdj and DBP1Adj at S and C band (see Figs. 10b,d), except for the most intense precipitation where it is still better. It is worth noticing that at S band the application of the adjustment coefficient results in an increase of the dispersion for large rainfall accumulation. At X band (Fig. 10f), the results are improved in all rainfall accumulation categories.

Overall, NB of DBP2 above 0.2-mm rainfall accumulation is kept within 0.2. Taking into consideration the representativeness of the uncertainties in the comparison between radar and rain gauges, this is a satisfactory result. The Z_h of the C- and X-band radars is likely to be underestimated, and the K_{dp} is not sensitive to radar calibration errors. Assuming the larger contribution to rainfall estimation at the >10 mm class is due to the R–K_{dp} estimator, it is obvious that the current R–K_{dp} relationship underestimates intense precipitation. This is very likely due to the applied range filtering. The high-frequency component of ϕ_{dp} is removed using a 6-km-long median filter. This is necessary to minimize the impact of phase noise on K_{dp} but it has the side effect of smoothing small convective cells, which results in this NB on the order of 0.1–0.2. To improve the results, either an adaptive range filtering or a change in K_{dp} coefficients should be implemented.

6. Conclusions

This paper has presented the new French operational polarimetric radar rainfall product. Currently, there is an operational product with two modes: one used by polarimetric radars (half of the network at the moment) and one used by conventional ones. The new product has several innovative features: it makes a wider use of polarimetry for echo classification and precipitation estimation. It attempts to improve the detectability level by providing a better noise-level estimation and by considering the impact of weaker ground clutter echoes. It

also addresses the issue of detectability by estimating the minimum detectable Z_h. Furthermore, it provides a dynamic estimation of the quality of the measurement by introducing the estimated attenuation as one of the parameters to determine the QI.

The new product is objectively evaluated against the previous product (in its polarimetric and nonpolarimetric modes) using hourly rain gauge accumulations. The results demonstrate the benefits of polarimetry, the added value of which increases at higher-frequency lengths. The first version of the polarimetric radar rainfall product, which essentially consists of filtering out clear-air echoes and correcting for precipitation-induced attenuation, already shows a considerable improvement of the scores, particularly for intense precipitation. The second version of the polarimetric radar rainfall product, which makes use of K_{dp} to estimate the rainfall rate, further improves the results.

Nevertheless, the results show some margin for improvement. Larger negative bias for intense precipitation at S band suggests that the attenuation correction applied at this band may be insufficient and therefore the attenuation coefficients should be revisited. The large bias presented by all products for the weakest precipitation may be partially due to measurement errors in the rain gauges. The capacity of the bucket is 0.2 mm; that is, a rainfall accumulation of 0.39 mm in 1 h would be accounted as 0.2 mm—almost 100% bias. Moreover, the uncertainty of the measurements is inversely proportional to the rainfall rate. Nevertheless, part of the positive bias can be attributed to the contribution of noise and collocated ground clutter in the Z_h. Such contributions should be removed. It is also evident that C- and X-band radars in the French network tend to underestimate Z_h. This may be partially due to wet radome attenuation [more severe at larger frequencies as stated in Frasier et al. (2012)], but miscalibration of the radar constant should not be excluded. Currently the radar receiver is calibrated using a signal source and overall radar performance is monitored by monthly comparisons with rain gauges. Monitoring using the self-consistency method (Gourley et al. 2009) and intercomparison between collocated radar gates may improve Z_h calibration. Although version two of the polarimetric radar rainfall product presents a better bias for intense precipitations, it still largely underestimates them. Uncertainties in the coefficients of the R–K_{dp} relationship may be partially blamed for that, but it is hypothesized that most of the underestimation is due to the smoothing of small but intense convective cells produced by the spatial filtering of ϕ_{dp}. An adaptive filter length would certainly improve the results.

The results of the new product on warm period precipitation are considered to be satisfactory. However, much more effort has to be placed on the processing of winter precipitation and hail cases. In this respect, the improved hydrometeor classification achieved by the use of polarimetry will certainly help. Robust relationships between the liquid water content of the various solid hydrometeor types and the polarimetric variables have to be established. It should also be noticed that the relationship between rain and polarimetric variables is not unequivocal, and the relationships we used are representative only of the most common drop size distribution in the region. Consequently, large deviations are possible. The real-time estimation of the DSD could be possible using the information provided by Z_{dr} but so far issues such as its stability, attenuation, and PBB have prevented its use in quantitative applications. Should the mentioned issues be tackled, an estimation of liquid water content on the ground based on the vertical profile of liquid water content could be provided, together with the minimum detectable liquid water content and the hydrometeor type on the ground.

Regardless of all the envisioned improvements on the rainfall estimation by individual radars, the issue of the optimal blending of data from different radars to obtain a national composite has not been discussed in this article. A specific study on how to combine data from polarimetric and nonpolarimetric radars and working at different frequency lengths is currently being conducted.

Finally, because the rainfall products were tested at the three wavelengths most commonly used for precipitation estimation (S, C, and X), these results provide some insight on the performance that can be expected from the different wavelengths. One should be aware, though, that the results are highly dependent on the measurement conditions. The relatively poor performance exhibited with the X-band measurements in particular are partly to blame on the difficult orographic conditions of the region where the radar is placed. However, the results exhibit a clear trend. Without correcting for precipitation-induced attenuation, the best performance is obtained at S band and the worst is obtained at X band by a large margin. The basic correction of attenuation largely reduces the differences in performance between the wavelengths, but the best performing are still the S-band measurements. The use of K_{dp}, which is insensitive to wet radome attenuation, further narrows the margin. Nevertheless, S band keeps providing the best performance. It can therefore be concluded that with the current state of technology single S-band radars are still the best performing in absolute terms although for a relatively narrow margin.

Acknowledgments. The financial support for this study was provided by the European Union, the Provence-Alpes-Côte d'Azur Region, and the French Ministry of Ecology, Energy, Sustainable Development and Sea through the RHYTMME project.

REFERENCES

Anagnostou, E. N., and W. Krajewski, 1999: Real-time radar rainfall estimation. Part I: Algorithm formulation. *J. Atmos. Oceanic Technol.,* **16,** 189–197.

Andrieu, H., and J. D. Creutin, 1995: Identification of vertical profiles of radar reflectivity for hydrological applications using an inverse method. Part I: Formulation. *J. Appl. Meteor.,* **34,** 225–239.

Beard, K. V., and C. Chuang, 1987: A new model for the equilibrium shape of raindrops. *J. Atmos. Sci.,* **44,** 1509–1524.

Brandes, E. A., G. Zhang, and J. Vivekanandan, 2002: Experiments in rainfall estimation with a polarimetric radar in a subtropical environment. *J. Appl. Meteor.,* **41,** 674–685.

——, ——, and ——, 2004: Comparison of polarimetric radar drop size distribution retrieval algorithms. *J. Atmos. Oceanic Technol.,* **21,** 584–598.

Bringi, V. N., and V. Chandrasekar, 2001: *Polarimetric Doppler Weather Radar*. Cambridge University Press, 636 pp.

——, T. D. Keenan, and V. Chandrasekar, 2001: Correcting C-band radar reflectivity and differential reflectivity data for rain attenuation: A self-consistent method with constraints. *IEEE Trans. Geosci. Remote Sens.,* **39,** 1906–1915.

——, M. A. Rico-Ramirez, and M. Thurai, 2011: Rainfall estimation with an operational polarimetric C-band radar in the U.K.: Comparison with a gauge network and error analysis. *J. Hydrometeor.,* **12,** 935–954.

Ciach, G. J., 2003: Local random errors in tipping-bucket rain gauge measurements. *J. Atmos. Oceanic Technol.,* **20,** 752–759.

Cocks, S. B., D. S. Berkowitz, R. Murnan, J. A. Schultz, S. Castleberry, K. Howard, K. Elmore, and S. Vasiloff, 2012: Initial assessment of the dual-polarization quantitative precipitation estimate algorithm's performance for two dual-polarization WSR-88Ds. *Proc. 28th Conf. on Interactive Information Processing Systems (IIPS),* New Orleans, LA, Amer. Meteor. Soc., 7B.2. [Available online at https://ams.confex.com/ams/92Annual/webprogram/Paper203568.html.]

Delrieu, G., J. D. Creutin, and H. Andrieu, 1995: Simulation of radar mountain returns using a digitized terrain model. *J. Atmos. Oceanic Technol.,* **12,** 1038–1049.

Didier, R., V. Ducrocq, and L. Auger, 2012: A climatology of the mesoscale environment associated with heavily precipitating events over a northwestern Mediterranean area. *J. Appl. Meteor. Climatol.,* **51,** 468–488.

Doviak, R. J., and D. S. Zrnic, 1993: *Doppler Radar and Weather Observations*. 2nd ed. Academic Press, 562 pp.

Emmanuel, I., H. Andrieu, and P. Tabary, 2012: Evaluation of the new French operational weather radar product for the field of urban hydrology. *Atmos. Res.,* **103,** 20–32.

Figueras i Ventura, J., A.-A. Boumahmoud, B. Fradon, P. Dupuy, and P. Tabary, 2012a: Long-term monitoring of French polarimetric radar data quality and evaluation of several polarimetric quantitative precipitation estimators in ideal conditions for operational implementation at C-band. *Quart. J. Roy. Meteor. Soc.,* **138,** 2212–2228.

——, P. Tabary, J. Sugier, M. Frech, and P. P. Alberoni, 2012b: Evaluation of new radar technologies: Operational monitoring and use of polarimetric C and S band radars. OPERA 3 WP 1.4b Rep. Ref. OPERA_2012_03, 57 pp.

Frasier, S., and Coauthors, 2012: Assessment of precipitation observations by a heterogeneous network of X- and K-band radars. *Proc. European Conf. on Radar in Meteorology and Hydrology, ERAD 2012,* Toulouse, France, Météo France, 5 pp. [Available online at http://www.meteo.fr/cic/meetings/2012/ERAD/extended_abs/NET_097_ext_abs.pdf.]

Fulton, R. A., J. P. Bredienbach, D.-J. Seo, D. A. Miller, and T. O'Bannon, 1998: The WSR-88 rainfall algorithm. *Wea. Forecasting,* **13,** 377–395.

Germann, U., and J. Joss, 2002: Mesobeta profiles to extrapolate radar precipitation measurements above the Alps to the ground level. *J. Appl. Meteor.,* **34,** 2612–2630.

Gourley, J. J., P. Tabary, and J. Parent du Chatelet, 2007a: A fuzzy logic algorithm for the separation of precipitating from nonprecipitating echoes using polarimetric radar observations. *J. Atmos. Oceanic Technol.,* **24,** 1439–1451.

——, ——, and ——, 2007b: Empirical estimation of attenuation from differential propagation phase measurements at C band. *J. Appl. Meteor. Climatol.,* **46,** 306–317.

——, A. J. Illingworth, and P. Tabary, 2009: Absolute calibration of radar reflectivity using redundancy of the polarization observations and implied constraints on drop shapes. *J. Atmos. Oceanic Technol.,* **26,** 689–703.

Gu, J.-Y., A. Ryzhkov, P. Zhang, P. Neilley, M. Knight, B. Wolf, and D.-I. Le, 2011: Polarimetric attenuation correction in heavy rain at C band. *J. Appl. Meteor. Climatol.,* **50,** 39–58.

Joss, J., and R. Lee, 1995: The application of radar–gauge comparisons to operational precipitation profile corrections. *J. Appl. Meteor.,* **34,** 2612–2630.

Kabeche, F., J. Figueras i Ventura, B. Fradon, A.-A. Boumahmoud, S. Frasier, and P. Tabary, 2012: Design and test of an X-band optimal rain rate estimator in the frame of the RHYTMME project. *Proc. European Conf. on Radar in Meteorology and Hydrology, ERAD 2012,* Toulouse, France, Météo France, 5 pp. [Available online at http://www.meteo.fr/cic/meetings/2012/ERAD/extended_abs/QPE_161_ext_abs.pdf.]

Kitchen, M., 1997: Towards improved radar estimates of surface precipitation rate at long range. *Quart. J. Roy. Meteor. Soc.,* **123,** 145–163.

Koistinen, J., 1991: Operational correction of radar rainfall errors due to the vertical reflectivity profile. *Proc. 25th Int. Conf. on Radar Meteorology,* Paris, France, Amer. Meteor. Soc., 91–94.

Maesaka, T., M. Maki, K. Iwanami, S. Tsuchiya, K. Kieda, and A. Hoshi, 2011: Operational rainfall estimation by X-band MP radar network in MLIT, Japan. *Proc. 35th Int. Conf. on Radar Meteorology,* Pittsburgh, PA, Amer. Meteor. Soc., 142. [Available online at https://ams.confex.com/ams/35Radar/webprogram/Paper191685.html.]

Marshall, J. S., R. C. Langille, and W. K. Palmer, 1947: Measurement of rainfall by radar. *J. Meteor.,* **4,** 186–192.

Parent du Chatelet, J., L. Perier, K. do Khack, and P. Roquain, 2001: CASTOR2: A new computer for the French radar network. *Proc. 30th Int. Conf. on Radar Meteorology,* Munich, Germany, Amer. Meteor. Soc., P2.14. [Available online at https://ams.confex.com/ams/pdfpapers/22195.pdf.]

Park, H. S., A. V. Ryzhkov, D. S. Zrnić, and K.-E. Kim, 2009: The Hydrometeor classification algorithm for the polarimetric

WSR-88D: Description and application to an MCS. *Wea. Forecasting,* **24,** 730–748.

Rico-Ramirez, M. A., 2012: Adaptive attenuation correction techniques for C-band polarimetric weather radars. *IEEE Trans. Geosci. Remote Sens.,* **50,** 5061–5071.

Ryzhkov, A., S. E. Giangrande, and T. J. Schuur, 2005: Rainfall estimation with a polarimetric prototype of WSR-88D. *J. Appl. Meteor.,* **44,** 502–515.

Seliga, T. A., and V. N. Bringi, 1976: Potential use of radar differential reflectivity measurements at orthogonal polarizations for measuring precipitation. *J. Appl. Meteor.,* **15,** 69–76.

Sugier, J., J. Parent du Chatelet, P. Roquain, and A. Smith, 2002: Detection and removal of clutter and anaprop in radar data using a statistical scheme based on echo fluctuation. *Proc. European Conf. on Radar in Meteorology and Hydrology,* Delft, Netherlands, ERAD, 17–24.

Tabary, P., 2007: The new French operational radar rainfall product. Part I: Methodology. *Wea. Forecasting,* **22,** 393–408.

——, G. Le Henaff, P. Dupuy, J. Parent du Chatelet, and J. Testud, 2008: Can we use polarimetric X-band radars for operational quantitative precipitation estimation in heavy rain regions? *Proc. Weather Radar and Hydrology Int. Symp.,* Grenoble, France, Laboratoire d'études des Transferts en Hydrologie et Environnement and L'Observatoire Hydro-météorologique Méditerranéen Cévennes-Vivarais, CD-ROM.

——, G. Vulpiani, J. J. Gourley, A. J. Illingworth, R. J. Thompson, and O. Bousquet, 2009: Unusually high differential attenuation at C band: Results from a two-year analysis of the French Trappes polarimetric radar data. *J. Appl. Meteor. Climatol.,* **48,** 2037–2053.

——, A.-A. Boumahmoud, H. Andrieu, R. J. Thompson, A. J. Illingworth, E. Le Bouar, and J. Testud, 2011: Evaluation of two ''integrated'' polarimetric Quantitative Precipitation Estimation (QPE) algorithms at C-band. *J. Hydrol.,* **405,** 248–260.

Tuttle, J. D., and G. B. Foote, 1990: Determination of boundary layer airflow from a single Doppler radar. *J. Atmos. Oceanic Technol.,* **7,** 218–232.

Zawadzki, I., 1984: Factors affecting the precision of radar measurements of rain. *Proc. 22nd Int. Conf. on Radar Meteorology,* Zurich, Switzerland, Amer. Meteor. Soc., 251–256.